PHYSICAL REVIEW A **90**, 041601(R) (2014)

Direct probe of topological order for cold atoms

Dong-Ling Deng,* Sheng-Tao Wang, and L.-M. Duan
Department of Physics, University of Michigan, Ann Arbor, Michigan 48109, USA
and Center for Quantum Information, IIIS, Tsinghua University, Beijing 100084, People's Republic of China
(Received 4 July 2014; published 6 October 2014)

Cold-atom experiments in optical lattices offer a versatile platform to realize various topological quantum phases. A key challenge in those experiments is to unambiguously probe the topological order. We propose a method to directly measure the characteristic topological invariants (order) based on the time-of-flight imaging of cold atoms. The method is generally applicable to detection of topological band insulators in one, two, or three dimensions characterized by integer topological invariants. Using detection of the Chern number for the two-dimensional anomalous quantum Hall states and the Chern-Simons term for the three-dimensional chiral topological insulators as examples, we show that the proposed detection method is practical, and robust to typical experimental imperfections such as limited imaging resolution, inhomogeneous trapping potential, and disorder in the system.

DOI: 10.1103/PhysRevA.90.041601 PACS number(s): 67.85.−d, 03.65.Vf, 37.10.Jk

The study of topological phases of matter, such as topological band insulators and superconductors, has attracted a lot of interest in recent years [1–3]. Various topological phases have been found associated with the free-fermion band theory and classified into a periodic table according to the system symmetry and dimensionality [4–6]. The topology of the band structure is characterized by a topological invariant taking only integer values, which gives the most direct and unambiguous signal of the corresponding topological order. To experimentally probe the topological order, it is desirable to have a way to measure the underlying topological invariant. For some phase, the topological invariant may manifest itself through certain quantized transport property or characteristic edge state behavior [7]. For instance, the quantized Hall conductivity is proportional to the underlying topological Chern number that characterizes the integer quantum Hall states [7–9]. For many other topological phases in the periodic table, it is not clear yet how to experimentally extract information of the underlying topological invariants.

Cold atoms in optical lattices provide a powerful experimental platform to simulate various quantum states of matter. In particular, recent experimental advance in engineering of spin-orbit coupling and artificial gauge field for cold atoms [10–15] has pushed this system to the forefront for realization of various topological quantum phases [16–22]. The detection method for cold-atom experiments is usually quite different from those for conventional solid-state materials. A number of intriguing proposals have been made for detection of certain topological order in cold-atom experiments, such as those based on the dynamic response [23–26], the Bragg spectroscopy [27,28], imaging of the edge states [29], counting peaks in the momentum distribution [30], or detection of the Berry phase or curvature [26,31–38]. Most of these proposals are targeted to detection of the quantum Hall phase. Similar to solid-state systems, it is not clear yet how to probe the topological invariants for various other topological phases in the periodic table.

In this Rapid Communication, we propose a general method to directly measure the topological invariants in cold-atom experiments based on the state-of-the-art time-of-flight (TOF) imaging. The TOF imaging, combined with the quench dynamics from the Hamiltonian, has been exploited in recent schemes for detection of the Chern numbers associated with two-band topological models in one- or two-dimensional optical lattices [26]. Compared with the previous work, our method has the following distinctive features: (1) it is applicable to detection of any topological band insulators with spin degrees of freedom in one, two, or three dimensions that are characterized by integer topological invariants in the periodic table. (2) The method is not limited by the requirement of a two-band structure for the Hamiltonian [26,31] or occupation of only the lowest band [33]. Instead, it detects the topological invariants associated with each band for any multiband Hamiltonians. (3) Our proposed detection method is very robust to practical experimental imperfections. As examples, we numerically simulate two experimental detections: one for the Chern number of the two-dimensional (2D) anomalous quantum Hall phase and the other for the Chern-Simons term of the three-dimensional (3D) chiral topological insulator. Both simulations show that accurate values of the topological invariants can be obtained experimentally under imaging resolution of a few to a dozen pixels along each spatial dimension, even with inhomogeneous traps and random potentials or interactions. The robustness is also found in Ref. [26] for detection of the Chern number in a different 2D model using the tomography method.

The topological band insulators are described by effective free-fermion Hamiltonians, typically with complicated spin-orbit couplings. We consider a real-space Hamiltonian with N spin (pseudospin) degrees of freedom, referred to as $|m\rangle$ with $m = 1,2,\ldots,N$. In the momentum $\mathbf{k}$ space, the Hamiltonian has N bands and is described by an N-by-N Hermitian matrix $H(\mathbf{k})$. The energy spectrum is obtained by solving the Schrödinger equation in the momentum space

$$H(\mathbf{k})|u_b(\mathbf{k})\rangle = E_b(\mathbf{k})|u_b(\mathbf{k})\rangle, \tag{1}$$

where $b = 1,2,\ldots,N$ is the band index and $|u_b(\mathbf{k})\rangle$ denotes the corresponding Bloch state with eigenenergy $E_b(\mathbf{k})$. For

*dldeng@umich.edu

simplicity, we assume the bands are nondegenerate. Expressed in the original spin basis $|m\rangle$, the Bloch state has the form

$$|u_b(\mathbf{k})\rangle = \sum_{m=1}^{N} c_{bm}(\mathbf{k})|m\rangle, \tag{2}$$

where $c_{bm}(\mathbf{k})$ is the Bloch wave function with normalization $\sum_m |c_{bm}(\mathbf{k})|^2 = 1$.

A topological invariant can be defined for each band, which usually takes the form of the Chern numbers for even spatial dimensions and the Chern-Simons terms (or the winding numbers in certain cases) for odd spatial dimensions. The Chern numbers (or Chern-Simons terms) can be expressed as momentum-space integrals of the Berry curvature and connection associated with the Bloch state $|u_b(\mathbf{k})\rangle$. For instance, in 2D (x,y plane), the Chern number C_b for the band b is defined by

$$C_b = -\frac{1}{2\pi}\int_{\mathrm{BZ}} dk_x dk_y F_{xy}^{(b)}(\mathbf{k}), \tag{3}$$

where the Berry curvature $F_{xy}^{(b)}(\mathbf{k}) \equiv \partial_{k_x} A_y^{(b)}(\mathbf{k}) - \partial_{k_y} A_x^{(b)}(\mathbf{k})$ and the Berry connection $A_\mu^{(b)}(\mathbf{k}) \equiv \langle u_b(\mathbf{k})| i\partial_{k_\mu}|u_b(\mathbf{k})\rangle (\mu = x,y)$, and the integration is over the whole Brillouin zone (BZ) which forms a compact manifold.

To probe the topological invariant such as the Chern number in Eq. (3), what we need to measure is the Bloch wave function $c_{bm}(\mathbf{k})$. The Berry connection and curvature can be obtained as derivatives of $c_{bm}(\mathbf{k})$ and the Chern number is just a twofold integration of $F_{xy}^{(b)}(\mathbf{k})$. For cold atoms in an optical lattice, we can map out the momentum distribution with the conventional time-of-flight imaging and separate different spin components through a magnetic field gradient [39]. Through the band mapping technique employed in experiments [17], populations in different bands are mapped to atomic densities in different spatial regions, so by this measurement we can get information about $n_{bm}(\mathbf{k}) = |c_{bm}(\mathbf{k})|^2$ for all occupied bands. To extract the wave function $c_{bm}(\mathbf{k})$, it is also crucial to measure the phase information. For this purpose, we apply an impulsive pulse right before the flight of atoms to induce a rotation between different spin components [40]. The rotation should keep the atomic momentum unchanged but mix their spins. For instance, a $\pi/2$ rotation between spin components m and m' induces the transition $c_{bm}(\mathbf{k}) \to [c_{bm}(\mathbf{k}) + c_{bm'}(\mathbf{k})]/\sqrt{2}$ and $c_{bm'}(\mathbf{k}) \to [-c_{bm}(\mathbf{k}) + c_{bm'}(\mathbf{k})]/\sqrt{2}$, which can be achieved by applying two copropagating Raman beams or a radio frequency pulse that couples the spin components m,m' and preserves the momentum $\mathbf{k}$. The pulse is short so that expansion of the atomic cloud is negligible during the pulse. For Raman pairs, relative phase coherence is kept but absolute phase locking is not necessary. The angular momentum change associated with the spin flip can be transferred from the Raman pair and selection rules have to be followed according to the specific atomic levels used. With this prior $\pi/2$ pulse, TOF imaging then measures the densities $|c_{bm}(\mathbf{k}) \pm c_{bm'}(\mathbf{k})|^2/2$, whose difference gives the interference terms $\mathrm{Re}[c_{bm}^*(\mathbf{k})c_{bm'}(\mathbf{k})]$. By the same method but with a different phase of the $\pi/2$ pulse, one can similarly measure the imaginary part $\mathrm{Im}[c_{bm}^*(\mathbf{k})c_{bm'}(\mathbf{k})]$ between any two spin components m and m'. The measurement of the population and interference terms $c_{bm}^*(\mathbf{k})c_{bm'}(\mathbf{k})$ for all m,m' fully determines the Bloch wave function $c_{bm}(\mathbf{k})$ up to arbitrariness of an overall phase $c_{bm}(\mathbf{k}) \to c_{bm}(\mathbf{k})e^{i\varphi(\mathbf{k})}$, where $\varphi(\mathbf{k})$ in general is $\mathbf{k}$ dependent but independent of the spin index.

In experiments, one needs to discretize the TOF image and measure the density distribution at each pixel of the BZ. The wave function $c_{bm}(\mathbf{k})$ is fixed up to an overall phase $\varphi(\mathbf{k})$ at each pixel with the above method. This arbitrary $\mathbf{k}$-dependent phase poses an obstacle to measurement of the topological invariants. To overcome this difficulty, we use a different way to calculate the Berry curvature based on the so-called $U(1)$ link defined for each pixel $\mathbf{k_J}$ of the discrete BZ [41]. The $U(1)$ link is defined as $U_\nu^{(b)}(\mathbf{k_J}) \equiv \langle u_b(\mathbf{k_J})|u_b(\mathbf{k_{J+\hat{\nu}}})\rangle/|\langle u_b(\mathbf{k_J})|u_b(\mathbf{k_{J+\hat{\nu}}})\rangle|$, where $\hat{\nu} = \hat{x},\hat{y},\hat{z}$, a unit vector in the corresponding direction. A gauge-independent field is obtained from the $U(1)$ link as [41]

$$\mathcal{F}_{\mu\nu}^{(b)}(\mathbf{k_J}) \equiv i \ln \frac{U_\mu^{(b)}(\mathbf{k_J})U_\nu^{(b)}(\mathbf{k_{J+\hat{\mu}}})}{U_\mu^{(b)}(\mathbf{k_{J+\hat{\nu}}})U_\nu^{(b)}(\mathbf{k_J})}, \tag{4}$$

where $\mathcal{F}_{\mu\nu}^{(b)}(\mathbf{k_J}) \in (-\pi,\pi]$ corresponds to a discrete version of the Berry curvature and it reduces to the latter in the large size limit. $\mathcal{F}_{\mu\nu}^{(b)}(\mathbf{k_J})$ can be obtained directly from the TOF images associated with the pixel $\mathbf{k_J}$ of the BZ, independent of the overall phase factor $\varphi(\mathbf{k})$. The topological invariant can be calculated from $\mathcal{F}_{\mu\nu}^{(b)}(\mathbf{k_J})$ by a direct summation over all the pixels of the BZ [instead of $\mathbf{k}$ integration in Eq. (3)]. This gives a simple and robust way to experimentally extract the topological invariant from the TOF images.

The detection method described above is general and applicable to various topological phases in different spatial dimensions. To show that the method is robust to experimental imperfections, in the following we numerically simulate detection of two kinds of topological invariants: one is the Chern number associated with the 2D quantum anomalous Hall effect and the other is the Chern-Simons term associated with the 3D chiral topological insulator.

2D quantum anomalous Hall (QAH) effect. The conventional quantum Hall effect requires application of a strong magnetic field. For the QAH effect, a combination of spontaneous magnetization and spin-orbit coupling gives rise to quantized Hall conductivity in the absence of an external magnetic field [42]. In solid-state systems, a recent experiment has observed this peculiar phenomenon in thin films of a magnetically doped topological insulator [43]. A simple square-lattice Hamiltonian which captures the essential physics of the QAH effect has the following form in real space:

$$\begin{aligned} H_{\mathrm{QAH}} = {} & \lambda_{\mathrm{SO}}^{(x)} \sum_{\mathbf{r}} [(a_{\mathbf{r}\uparrow}^\dagger a_{\mathbf{r}+\hat{x}\downarrow} - a_{\mathbf{r}\uparrow}^\dagger a_{\mathbf{r}-\hat{x}\downarrow}) + \mathrm{H.c.}] \\ & + i\lambda_{\mathrm{SO}}^{(y)} \sum_{\mathbf{r}} [(a_{\mathbf{r}\uparrow}^\dagger a_{\mathbf{r}+\hat{y}\downarrow} - a_{\mathbf{r}\uparrow}^\dagger a_{\mathbf{r}-\hat{y}\downarrow}) + \mathrm{H.c.}] \\ & - t \sum_{\langle \mathbf{r},\mathbf{s}\rangle} (a_{\mathbf{r}\uparrow}^\dagger a_{\mathbf{s}\uparrow} - a_{\mathbf{r}\downarrow}^\dagger a_{\mathbf{s}\downarrow}) + h \sum_{\mathbf{r}} (a_{\mathbf{r}\uparrow}^\dagger a_{\mathbf{r}\uparrow} - a_{\mathbf{r}\downarrow}^\dagger a_{\mathbf{r}\downarrow}), \end{aligned} \tag{5}$$

where $a_{\mathbf{r}\sigma}^\dagger$ ($a_{\mathbf{r}\sigma}$) is the creation (annihilation) operator of the fermionic atom with pseudospin $\sigma = (\uparrow,\downarrow)$ at site $\mathbf{r}$, and $\hat{x},\hat{y}$ are unit lattice vectors along the x,y directions. The first term in

the Hamiltonian describes the spin-orbit coupling. The second and the third terms denote, respectively, the spin-conserved nearest-neighbor hopping and the Zeeman interaction. It was proposed recently that $H_{\rm QAH}$ may be realized with cold fermionic atoms trapped in a blue-detuned optical lattice [44].

In momentum space, this Hamiltonian has two Bloch bands. The topological structure of this model is characterized by the Chern number defined in Eq. (3). Direct calculation shows that $C_2 = -C_1 = \mathrm{sgn}(h)$ when $0 < |h| < 4t$ and $C_2 = -C_1 = 0$ otherwise. Experimentally, one can measure $\mathcal{F}^{(b)}_{\mu\nu}(\mathbf{k_J})$ by our proposed method to extract the Chern number through $C_b \approx -\sum_{\mathbf{J}} \mathcal{F}^{(b)}_{xy}(\mathbf{k_J})/(2\pi)$, where the band index $b = 1,2$.

To simulate experiments, we consider a finite-size lattice with open boundary condition. In addition, we add a global harmonic trap of the form $V_T = m_a\omega^2 r^2/2$ for atoms of mass m_a as in real experiments and use $\gamma_T = m_a\omega^2 a^2/2t$ to parametrize the relative strength of the trap, where a denotes the lattice constant. To account for possible experimental noise, we add a random perturbation Hamiltonian of the following general form

$$H_{\rm P} = \gamma_{\rm P} t \sum_{\langle \mathbf{r},\mathbf{s}\rangle,\alpha,\beta} a^\dagger_{\mathbf{r},\alpha} \mathcal{P}_{\mathbf{r}\alpha,\mathbf{s}\beta} a_{\mathbf{s},\beta}, \tag{6}$$

where $\gamma_{\rm P}$ is a dimensionless parameter characterizing the strength of random perturbation, $\langle \mathbf{r},\mathbf{s}\rangle$ denotes the neighboring sites, and $\mathcal{P}$ is a random Hermitian matrix with its largest eigenvalue normalized to unity. We numerically diagonalize the real-space Hamiltonian on a finite lattice with different number of sites and calculate the corresponding momentum density distributions [45]. An an example, in Fig. 1, we show the reconstructed density distribution in two complementary bases ($\{|\uparrow\rangle,|\downarrow\rangle\}$, $\{|\uparrow\rangle \pm |\downarrow\rangle\}$) under open boundary condition with a harmonic trap and random perturbations (more detailed calculation results are shown in the Supplemental Material [45]). The Chern numbers for each case are calculated and listed in Table I under choices of different parameters and system sizes. The extracted Chern numbers exactly equal the corresponding theoretical values, even under a small system size and significant disorder potentials. This is so as Chern numbers characterize the topological property,

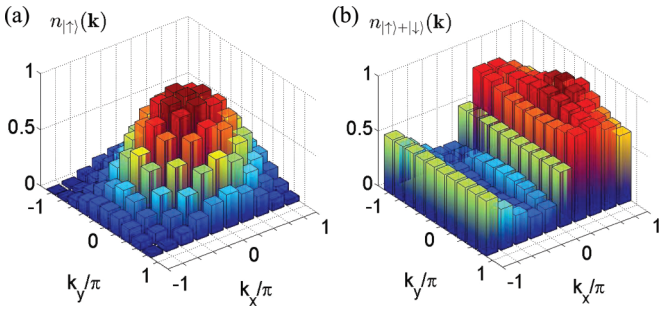

FIG. 1. (Color online) Density distributions in momentum space for the first band of $H_{\rm QAH}$ under two different spin bases with lattice size 10×10 and open boundary condition. The total density at each $\mathbf{k}$ is normalized to unity [e.g., $n_{|\uparrow\rangle}(\mathbf{k}) + n_{|\downarrow\rangle}(\mathbf{k}) = 1$] corresponding to the unit filling. The parameters are chosen to be $\lambda^{(x)}_{\rm SO} = \lambda^{(y)}_{\rm SO} = h = t$, $\gamma_T = 0.01t$, and $\gamma_P = 0.1t$.

TABLE I. Simulated detection results of the topological invariants for different lattice sizes under various conditions (periodic boundary condition, open boundary condition, with trap, with both trap and perturbation Hamiltonians). For the QAH, the invariant is the Chern number for the first band (C_1), whereas for the CTI, it is the Chern-Simons term for the middle flat band (CS_2/π). Results for both the nontrivial phase ($h/t = 1$ for the QAH and $h/t = 2$ for the CTI) and the trivial phase ($h/t = 5$ for the QAH and $h/t = 4$ for the CTI) are presented. The parameters are the same as in Figs. 1 and 2.

	h/t	Size	Periodic	Open	Trap	Pert.+trap
QAH	1	4^2	-1	-1	-1	-1
	1	10^2	-1	-1	-1	-1
	5	10^2	0	0	0	0
CTI	2	10^3	1.041	1.056	1.055	1.080
	2	12^3	1.031	1.009	0.981	1.014
	4	10^3	0	-2×10^{-4}	1.1×10^{-3}	1.2×10^{-3}

which does not change under perturbations. Furthermore, our detection method through measurement of $\mathcal{F}^{(b)}_{\mu\nu}(\mathbf{k_J})$ guarantees an integer value for the extracted Chern number [41], so it automatically corrects small errors due to experimental imperfections. Reference [26] also points out the robustness of the method of Fukui *et al.* [41] in computing the Chern number.

3D chiral topological insulator. Chiral topological insulators (CTIs) are protected by the chiral symmetry (also known as the sublattice symmetry) and belong to the AIII class in the periodic table for topological phases [4–6]. A simple Hamiltonian that supports 3D CTIs has the form [46]

$$H_{\rm CTI} = \frac{t}{2}\sum_{\mathbf{r}}\sum_{j=1}^{3}[\psi^\dagger_{\mathbf{r}}(iG_{3+j} - G_7)\psi_{\mathbf{r}+\mathbf{e}_j} + \mathrm{H.c.}] + h\sum_{\mathbf{r}}\psi^\dagger_{\mathbf{r}} G_7 \psi_{\mathbf{r}}, \tag{7}$$

where the operator $\psi^\dagger_{\mathbf{r}} = (a^\dagger_{\mathbf{r},1}, a^\dagger_{\mathbf{r},2}, a^\dagger_{\mathbf{r},3})$ with $a^\dagger_{\mathbf{r},\alpha}$ ($\alpha = 1,2,3$) creating a fermion at site $\mathbf{r}$ with spin state α, $\mathbf{e}_1,\mathbf{e}_2,\mathbf{e}_3$ are unit vectors along the x,y,z directions, and G_ν ($\nu = 4,5,6,7$) denotes the νth Gell-Mann matrix [45]. In the momentum space, this model Hamiltonian has three gapped bands, with a zero-energy flat band in the middle protected by the chiral symmetry. An experimental scheme has been proposed to realize this model Hamiltonian with cold fermionic atoms in an optical lattice [47]. The topological property of this Hamiltonian can be described by the Chern-Simons term. For the bth ($b = 1,2,3$) Bloch band, the Chern-Simons term CS_b takes the form

$$\mathrm{CS}_b = \frac{1}{4\pi}\int_{\rm BZ} d\mathbf{k}\epsilon^{\mu\nu\tau} A^{(b)}_\mu(\mathbf{k})\partial_{k_\nu} A^{(b)}_\tau(\mathbf{k}), \tag{8}$$

where $A^{(b)}_\mu(\mathbf{k}) = \langle u_b(\mathbf{k})|i\partial_{k_\mu}|u_b(\mathbf{k})\rangle (\mu = x,y,z)$. Explicit calculations show that $\mathrm{CS}_3 = \mathrm{CS}_1 = \mathrm{CS}_2/4 = \pi\Gamma(h)/4$ with $\Gamma(h) = -2$ for $|h| < t$, $\Gamma(h) = 1$ for $t < |h| < 3t$, and $\Gamma(h) = 0$ otherwise.

As an example application of our general detection method, here we show how to measure the topological invariant CS_b through the TOF imaging. As shown in Fig. 2(a), we first use

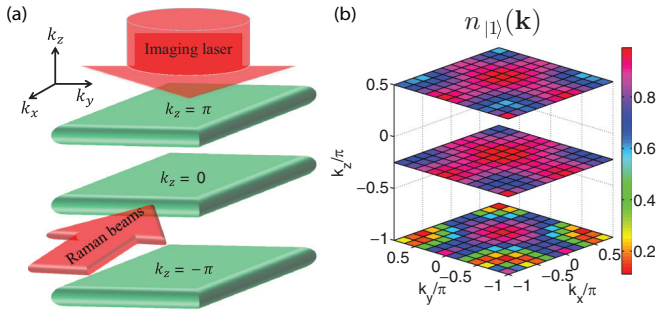

FIG. 2. (Color online) (a) An illustration to show reconstruction of the 3D atomic momentum distribution by the TOF imaging. (b) Momentum distribution in one particular spin basis (other results are shown in the Supplemental Material [45]) for the middle flat band of H_{CTI} with open boundary condition under lattice size $12 \times 12 \times 12$. Layers corresponding to $k_z = -\pi, -\pi/4, \pi/2$ are displayed. The parameters are $h = 2t$, $\gamma_T = 0.001t$, and $\gamma_P = 0.1t$.

the TOF imaging to reconstruct the 3D atomic momentum distribution. After expansion of the atomic cloud, we apply a pair of copropagating Raman beams focused in the z axis to transfer a layer of atoms with a fixed z coordinate z_i to another hyperfine or Zeeman level denoted as $|r\rangle$. We apply the imaging laser to couple the atoms only on the $|r\rangle$ level, so the imaging reads out the 2D momentum distribution $n(k_x, k_y, k_{z_i})$ with a fixed $k_{z_i} \propto z_i$. We repeat this measurement by scanning the coordinate z_i so that each image gives a 2D distribution $n(k_x, k_y, k_{z_i})$ with a different k_{z_i}. By this method, we reconstruct the 3D momentum distribution $n(k_x, k_y, k_z)$, where l images give l pixels of k_z.

To extract the Chern-Simons term CS_b, we measure the 3D momentum distribution $n_{bm}(k_x, k_y, k_z)$ in different spin bases to obtain the Bloch wave function $c_{bm}(\mathbf{k})$. We then use the measured $c_{bm}(\mathbf{k})$ to calculate the gauge-independent field $\mathcal{F}^{(b)}_{\mu\nu}(\mathbf{k_J})$ defined in Eq. (4). By solving a discrete version of the equation $\nabla \times \mathbf{A} = \mathbf{F}$ in the momentum space with the Coulomb gauge $\nabla \cdot \mathbf{A} = 0$, we obtain the Berry connection $A^{(b)}_{\mu}(\mathbf{k_J})$ from $\mathcal{F}^{(b)}_{\mu\nu}(\mathbf{k_J})$. With $A^{(b)}_{\mu}$, we extract the Chern-Simons term CS_b using Eq. (8).

The Chern-Simons terms extracted from our numerically simulated experiments are shown in Table I under various conditions. Different from the Chern number case, extraction of the Chern-Simons term using Eq. (8) does not guarantee the result to be an integer, so the calculated values are subject to the influence of numerical inaccuracies and experimental noise. Nevertheless, from the results listed in Table I, we see that the extracted values quickly approach the corresponding theoretical limits when we take a dozen of the pixels along each spatial dimension in the time-of-flight imaging and the detection method remains robust to experimental imperfections (traps and random perturbation Hamiltonians change the result by less than 3%).

In summary, we have proposed a general method to experimentally measure the topological invariants for ultracold atoms. The method is shown to be robust to various experimental imperfections through numerically simulated experiments.

We thank S.-L. Zhu for discussions. This work was supported by the NBRPC (973 Program) Grants No. 2011CBA00302, the IARPA MUSIQC program, the ARO, and the AFOSR MURI program.

[1] M. Z. Hasan and C. L. Kane, Rev. Mod. Phys. **82**, 3045 (2010).
[2] X.-L. Qi and S.-C. Zhang, Rev. Mod. Phys. **83**, 1057 (2011).
[3] J. E. Moore, Nature (London) **464**, 194 (2010).
[4] A. P. Schnyder, S. Ryu, A. Furusaki, and A. W. W. Ludwig, Phys. Rev. B **78**, 195125 (2008).
[5] A. Kitaev, AIP Conf. Proc. **1134**, 22 (2009).
[6] S. Ryu, A. P. Schnyder, A. Furusaki, and A. W. Ludwig, New J. Phys. **12**, 065010 (2010).
[7] D. J. Thouless, M. Kohmoto, M. P. Nightingale, and M. den Nijs, Phys. Rev. Lett. **49**, 405 (1982).
[8] K. von Klitzing, Rev. Mod. Phys. **58**, 519 (1986).
[9] S. D. Sarma and A. Pinczuk, *Perspectives in Quantum Hall Effects* (Wiley, New York, 2008).
[10] Y.-J. Lin, R. L. Compton, K. Jimenez-Garcia, J. V. Porto, and I. B. Spielman, Nature (London) **462**, 628 (2009).
[11] X.-J. Liu, M. F. Borunda, X. Liu, and J. Sinova, Phys. Rev. Lett. **102**, 046402 (2009).
[12] P. Wang, Z.-Q. Yu, Z. Fu, J. Miao, L. Huang, S. Chai, H. Zhai, and J. Zhang, Phys. Rev. Lett. **109**, 095301 (2012).
[13] L. W. Cheuk, A. T. Sommer, Z. Hadzibabic, T. Yefsah, W. S. Bakr, and M. W. Zwierlein, Phys. Rev. Lett. **109**, 095302 (2012).
[14] J. Dalibard, F. Gerbier, G. Juzeliūnas, and P. Öhberg, Rev. Mod. Phys. **83**, 1523 (2011).
[15] V. Galitski and I. B. Spielman, Nature (London) **494**, 49 (2013).
[16] M. Lewenstein, A. Sanpera, V. Ahufinger, B. Damski, A. Sen, and U. Sen, Adv. Phys. **56**, 243 (2007).
[17] I. Bloch, J. Dalibard, and S. Nascimbène, Nat. Phys. **8**, 267 (2012).
[18] S.-L. Zhu, H. Fu, C.-J. Wu, S.-C. Zhang, and L.-M. Duan, Phys. Rev. Lett. **97**, 240401 (2006).
[19] S.-L. Zhu, L.-B. Shao, Z. D. Wang, and L.-M. Duan, Phys. Rev. Lett. **106**, 100404 (2011).
[20] B. Béri and N. R. Cooper, Phys. Rev. Lett. **107**, 145301 (2011).
[21] M. Aidelsburger, M. Atala, M. Lohse, J. T. Barreiro, B. Paredes, and I. Bloch, Phys. Rev. Lett. **111**, 185301 (2013).
[22] H. Miyake, G. A. Siviloglou, C. J. Kennedy, W. C. Burton, and W. Ketterle, Phys. Rev. Lett. **111**, 185302 (2013).
[23] L. B. Shao, S.-L. Zhu, L. Sheng, D. Y. Xing, and Z. D. Wang, Phys. Rev. Lett. **101**, 246810 (2008).
[24] A. Dauphin and N. Goldman, Phys. Rev. Lett. **111**, 135302 (2013).
[25] L. Wang, A. A. Soluyanov, and M. Troyer, Phys. Rev. Lett. **110**, 166802 (2013).
[26] P. Hauke, M. Lewenstein, and A. Eckardt, Phys. Rev. Lett. **113**, 045303 (2014).
[27] X.-J. Liu, X. Liu, C. Wu, and J. Sinova, Phys. Rev. A **81**, 033622 (2010).

[28] N. Goldman, J. Beugnon, and F. Gerbier, Phys. Rev. Lett. **108**, 255303 (2012).
[29] N. Goldman, J. Dalibard, A. Dauphin, F. Gerbier, M. Lewenstein, P. Zoller, and I. B. Spielman, Proc. Natl. Acad. Sci. USA **110**, 6736 (2013).
[30] E. Zhao, N. Bray-Ali, C. J. Williams, I. B. Spielman, and I. I. Satija, Phys. Rev. A **84**, 063629 (2011).
[31] E. Alba, X. Fernandez-Gonzalvo, J. Mur-Petit, J. K. Pachos, and J. J. García-Ripoll, Phys. Rev. Lett. **107**, 235301 (2011).
[32] H. M. Price and N. R. Cooper, Phys. Rev. A **85**, 033620 (2012).
[33] X.-J. Liu, K. T. Law, T. K. Ng, and P. A. Lee, Phys. Rev. Lett. **111**, 120402 (2013).
[34] D. A. Abanin, T. Kitagawa, I. Bloch, and E. Demler, Phys. Rev. Lett. **110**, 165304 (2013).
[35] M. Atala, M. Aidelsburger, J. T. Barreiro, D. Abanin, T. Kitagawa, E. Demler, and I. Bloch, Nat. Phys. **9**, 795 (2013).
[36] N. Goldman, E. Anisimovas, F. Gerbier, P. Öhberg, I. B. Spielman, and G. Juzeliūnas, New J. Phys. **15**, 013025 (2013).
[37] J. K. Pachos, E. Alba, V. Lahtinen, and J. J. Garcia-Ripoll, Phys. Rev. A **88**, 013622 (2013).
[38] J. de Lisle, S. De, E. Alba, A. Bullivant, J. J. Garcia-Ripoll, V. Lahtinen, and J. K. Pachos, New J. Phys. **16**, 083022 (2014).
[39] W. Ketterle and M. Zwierlein, Riv. Nuovo Cimento **31**, 247 (2008).
[40] L.-M. Duan, Phys. Rev. Lett. **96**, 103201 (2006).
[41] T. Fukui, Y. Hatsugai, and H. Suzuki, J. Phys. Soc. Jpn. **74**, 1674 (2005).
[42] F. D. M. Haldane, Phys. Rev. Lett. **61**, 2015 (1988).
[43] C.-Z. Chang, J. Zhang, X. Feng, J. Shen, Z. Zhang, M. Guo, K. Li, Y. Ou, P. Wei, L.-L. Wang *et al.*, Science **340**, 167 (2013).
[44] X.-J. Liu, K. T. Law, and T. K. Ng, Phys. Rev. Lett. **112**, 086401 (2014).
[45] See Supplemental Material at http://link.aps.org/supplemental/10.1103/PhysRevA.90.041601 for more details on the calculations of the momentum density distributions and more plots of the numerical simulations.
[46] T. Neupert, L. Santos, S. Ryu, C. Chamon, and C. Mudry, Phys. Rev. B **86**, 035125 (2012).
[47] S.-T. Wang, D.-L. Deng, and L.-M. Duan, Phys. Rev. Lett. **113**, 033002 (2014).